Chin. Sci. Bull. (2014) 59(2):190–200
DOI 10.1007/s11434-013-0055-y csb.scichina.com

Article Geography

Relative humidity reconstruction for northwestern China's Altay Mountains using tree-ring $\delta^{18}O$

Guobao Xu · Xiaohong Liu · Dahe Qin · Tuo Chen · Wenzhi Wang · Guoju Wu · Weizhen Sun · Wenling An · Xiaomin Zeng

Received: 6 May 2013 / Accepted: 15 August 2013 / Published online: 31 December 2013

Abstract Relative humidity is an important factor in water and water vapor feedback cycles. In this study, we established a 222-year annual tree-ring $\delta^{18}O$ chronology for Siberian larch (*Larix sibirica* Ldb.) from the Altay Mountains in northwestern China. Climate response analyses revealed that the relative humidity was the primary factor limiting tree-ring $\delta^{18}O$ fractionation. Based on our analysis, tree-ring $\delta^{18}O$ can be used to reconstruct the July–August relative humidity based on both a reasonable mechanism of tree-ring $\delta^{18}O$ fractionation and a statistically significant regression model. We used this model to reconstruct variations in the July–August relative humidity, and the model explained 47.4 % of the total variation in the measured relative humidity data from 1961 to 2011. The relative humidity in the study area increased from 1900 to the 1990s and decreased thereafter. Two regime-shift dry periods were detected during the study period (one from 1817 to 1830 and the other from 2004 to 2011).

Keywords Tree-ring $\delta^{18}O$ · Relative humidity · Altay Mountains · Siberian larch · Regime shift

G. Xu · X. Liu (✉) · D. Qin · T. Chen · W. Wang · G. Wu · W. Sun · W. An · X. Zeng
State Key Laboratory of Cryospheric Sciences, Cold and Arid Regions Environmental and Engineering Research Institute, Chinese Academy of Sciences, Lanzhou 730000, China
e-mail: liuxh@lzb.ac.cn

G. Xu · W. Wang · G. Wu · W. An · X. Zeng
College of Resources and Environment, University of Chinese Academy of Sciences, Beijing 100049, China

G. Xu
Institute of Desert Meteorology, China Meteorological Administration, Ürümqi 830002, China

1 Introduction

Relative humidity is an important factor for water and water vapor feedback cycles and for the energy balance of the atmosphere system. For example, the feedback between water vapor and clouds depends strongly on changes in the relative humidity [1, 2]. Relative humidity is also a vital factor that determines the balance of water and gas exchange during plant transpiration and photosynthetic assimilation [3, 4]. It directly influences plant water relations and indirectly affects leaf growth, photosynthesis, shoot growth, disease occurrence, and the economic yield of crops, among other factors [5–8]. Thus, relative humidity is an essential factor in studies of climatology and plant ecology.

However, relative humidity is one of the most difficult environmental factors to monitor [7]. Although accurate and relatively simple instantaneous measurement is feasible, continuous humidity measurements were not available for most locations in northwestern China until the late 1950s. Long-term knowledge of the variability of relative humidity is beneficial for assessing the historical variability of regional water systems, hydrology, and plant ecology in arid and semiarid areas such as northwestern China. Based on a tree-ring isotopic model, $\delta^{18}O$ in tree rings can potentially record the variability of relative humidity. Tree-ring $\delta^{18}O$ values are primarily controlled by the meteoric (source) water availability and by isotopic enrichment in leaf water [9, 10]. The $\delta^{18}O$ in leaf water is enriched in ^{18}O by transpiration at low relative humidity and depleted at high relative humidity [11–13]. Since relative humidity strongly controls stomatal conductance, tree-ring cellulose $\delta^{18}O$ is affected by the stomatal aperture [9, 14], and preserves information on the relative humidity conditions when plant tissues that incorporate ^{18}O formed.

The Craig–Gordon model for isotopic fractionation has been modified for use as a tree-ring δ^{18}O model [15]:

$$\delta^{18}\mathrm{O}_{\mathrm{cell}} = (1 - f_{\mathrm{o}})\left[\delta^{18}\mathrm{O}_{\mathrm{s}} + (\varepsilon_{\mathrm{e}} + \varepsilon_{\mathrm{k}})(1 - h) + \varepsilon_{\mathrm{o}}\right] + f_{\mathrm{o}}\left(\delta^{18}\mathrm{O}_{\mathrm{s}} + \varepsilon_{\mathrm{o}}\right), \quad (1)$$

where $\delta^{18}\mathrm{O}_{\mathrm{cell}}$ and $\delta^{18}\mathrm{O}_{\mathrm{s}}$ are the δ^{18}O in the tree-ring cellulose and the source water, respectively. f_{o} is a damping factor, ε_{e} is the equilibrium fractionation factor, ε_{k} is the kinetic fractionation factor, h is the relative humidity, and ε_{o} is the biochemical fractionation factor.

According to the tree-ring δ^{18}O model [9, 10, 15, 16], variation in the relative humidity leaves a fingerprint in the tree-ring δ^{18}O. The tree-ring δ^{18}O has, therefore, been used as a potential tool to detect the variations in relative humidity [17–23].

Herein, we report the results of a study designed to develop a proxy for seasonal relative humidity in the Altay Mountains of northwestern China using the δ^{18}O values in tree-ring cellulose. We reconstructed the relative humidity from 1790 to 2011 using the resulting model, and analyzed the variations in relative humidity in terms of their trends, regime shifts, and extreme years. We then compared our reconstruction with several other regional moisture environment reconstructions to validate our results.

2 Materials and methods

2.1 Climate of the study area

The study area is located in the Altay Mountains region of northwestern China (Fig. 1). We based our analysis on climatic records from the Fuyun meteorological station (46.98°N, 89.52°E, 826.6 m a.s.l), which is the station nearest to the sampling site (about 60 km). The data were obtained from the Chinese meteorological data center (http://www.cma.gov.cn/2011qxfw/2011qsjgx/). We tested the records for homogeneity using the standard normal homogeneity test [24] and found no abrupt changes. The climatic parameters in our analysis included monthly temperatures (maximum, minimum, and mean), the monthly total precipitation, and the mean monthly relative humidity from 1961 to 2011. The climate records from the Fuyun station showed that the study region has a cool climate with a multi-year mean annual temperature of 3.0 °C. January (with a monthly mean temperature of −21.6 °C) and July (22.2 °C) are the coldest and warmest months, respectively (Fig. 2a). The total annual precipitation is 190 mm, and the two wettest months are July and November. The average annual relative humidity is 59.2 %, with higher values from January to March (mean 74.5 %) and from November to December (mean 75.1 %).

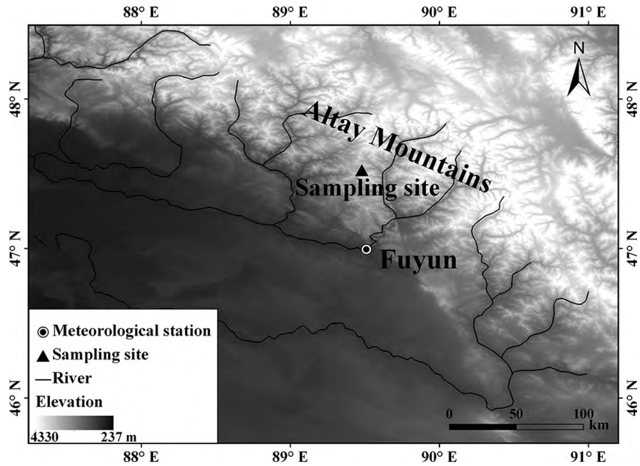

Fig. 1 Location of the sampling site and meteorological station

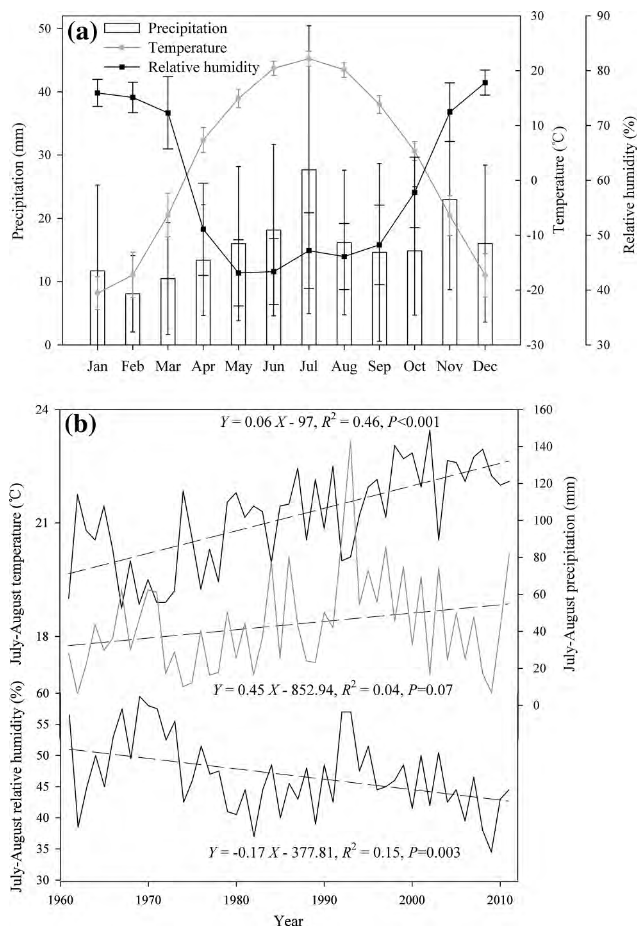

Fig. 2 **a** Climate of the study area (values are mean ± standard deviations); **b** the variations of July–August mean temperature, precipitation, and relative humidity from 1961 to 2011. *Dashed lines* represent linear regressions between the climatic parameters and time

From May to September, the relative humidity averages around 45.6 % and about 48.7 % of the total annual precipitation are received during this period. Figure 2b shows that since 1961, the July–August temperature in the area has increased significantly (0.6 °C/decade, $P < 0.001$) while relative humidity has decreased significantly (−1.7 %/decade, $P = 0.003$). July–August precipitation showed a slow and only marginally significant increase overall, but showed a decreasing trend from 1990 to 2011.

2.2 Sampling and cross-dating

Siberian larch (*Larix sibirica* Ldb.) is a dominant tree species at altitudes from 1,400 to 2,400 m a.s.l. in the Altay Mountains. This species has strong resistance to both cold and drought. The Siberian larch forms surface root systems as well as adventitious roots; therefore, it has a shallow root system [25]. In the study area, the larch begins its growth in May, enters a period of fast growth during June and July, and becomes dormant beginning in September [26]. The larch forms mixed stands with a crown cover of 10 % to 15 % and a distance of about 10 m between trees at the sampling site (47.52°N, 89.48°E; Fig. 1). The soil is characterized by a relatively small stone content and a moderate amount of clay. The source water for the Siberian larch is primary from the summer precipitation and less from snow [27]. The $\delta^{18}O$ of source water (soil water) of tree has an important role for the tree-ring $\delta^{18}O$ [9, 15], but no data of source water $\delta^{18}O$ are available to discuss this issue here.

We collected 32 tree-ring cores (two cores per tree) from larch growing at altitudes ranging from 2,090 to 2,140 m a.s.l at the upper tree-line using a 12-mm-diameter increment borer (Haglöf, Mora, Sweden) at breast height (about 1.3 m above the ground) in August 2011. All cores were air-dried and then polished using progressively finer grades of sandpaper in the laboratory. After the cellular structure had been clearly revealed, all cores were visually cross-dated using a standard methodology [28]. We measured all cross-dated growth rings to a precision of 0.01 mm using a sliding stage micrometer (LINTAB 6; Rinntech, Heidelberg, Germany) interfaced with a computer using the time series analysis and presentation features of the device's dendrochronological software. The quality of cross-dating was confirmed using the COFECHA software [29] (http://www.ncdc.noaa.gov/paleo/treering/cofecha/cofecha.html). The oldest tree was older than 522 years (i.e., the core did not pass through the pith, so this is a minimum age). The mean sensitivity for the width chronology was 0.242.

2.3 Tree-ring isotope analysis

We selected nine cores (one core per tree) from trees with homogeneous growth patterns and few or no missing years to obtain enough wood materials. We discarded the initial 30 years of each core to avoid the potential juvenile effect [10, 30, 31]. Many rings were narrow or had indistinct latewood, so we used the whole wood from each year for α-cellulose extraction. We then pooled the annual wood samples prior to α-cellulose extraction [32, 33]. We first milled the pooled annual samples (<80 μm), and then extracted α-cellulose using methods of Loader et al. [34] and Liu et al. [35]. To better homogenize the cellulose, we used an ultrasound machine (JY92-2D, Scientz Industry, Ningbo, China) to break the cellulose fibers, following the method of Laumer et al. [36].

For the $\delta^{18}O$ measurements, we loaded 0.14–0.16 mg of α-cellulose into silver capsules, and determined the ratio using a High Temperature Conversion Elemental Analyzer coupled to a Finnigan MAT-253 mass spectrometer (Thermo Electron Corporation, Bremen, Germany) at the State Key Laboratory of Cryospheric Sciences, Chinese Academy of Sciences. Samples for $\delta^{18}O$ ratio measurements were pyrolyzed to CO at 1,350 °C operating in the continuous flow mode. The $\delta^{18}O$ analyses were repeated four times for each annual cellulose sample. After excluding the outliers (values more than three σ from the mean), we calculated the mean values. We also calculated the standard deviation of each sample, and used this parameter to represent the measurement uncertainty for each sample (Fig. 3a). We measured the ratio for a benzoic acid working standard with a known $\delta^{18}O$ value (IAEA-601, 23.3 ‰) every seven measurements to monitor the analytical precision and to calibrate the samples for analytical accuracy. We also used the cellulose standard IAEA-C_3 (32.2 ‰) to calibrate the tree-ring $\delta^{18}O$ measurements. The mean analytical uncertainty was 0.17 ‰ (1 σ) for $\delta^{18}O$. Based on the suggestion that the mean $\delta^{18}O$ of a minimum of six cores can reliably represent the site $\delta^{18}O$ chronology for larch [30], the $\delta^{18}O$ isotope data that met this criterion covered the period from 1790 to 2011, and we chose this period for further analysis (Fig. 3b).

2.4 Statistical analysis and transfer function

To investigate the climate signals recorded in the tree-ring $\delta^{18}O$ series, we calculated Pearson's correlation (r) and partial correlations between tree-ring $\delta^{18}O$ and the climatic variables. Bootstrap resampling methods [37, 38] were applied to verify the reliability and stability of these correlations. The window for the response of tree-ring $\delta^{18}O$ to climate spanned the period from September of the previous year to October of the current year. We estimated a transfer function by means of linear regression and estimated the reconstruction uncertainties based on the resulting linear model and $\delta^{18}O$ measurement uncertainties. We used leave-one-out validation [39] to verify our reconstruction because the dataset from 1961 to 2011 (51 years) was too short to divide into two subsets that would allow

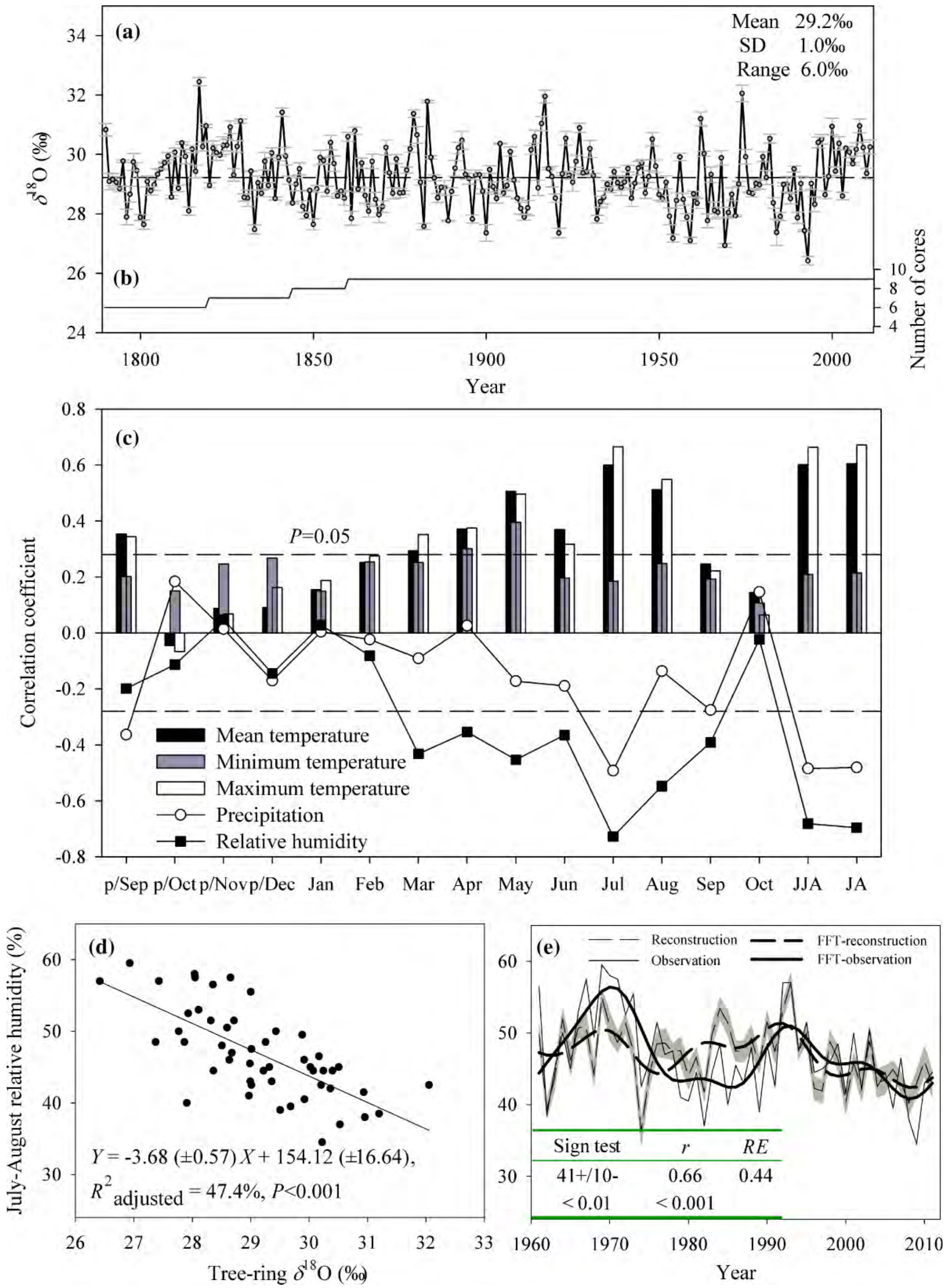

(a)
Mean 29.2‰
SD 1.0‰
Range 6.0‰
δ^{18}O (‰)
(b)
Number of cores
Year
(c)
P=0.05
Correlation coefficient
Mean temperature
Minimum temperature
Maximum temperature
Precipitation
Relative humidity
p/Sep p/Oct p/Nov p/Dec Jan Feb Mar Apr May Jun Jul Aug Sep Oct JJA JA
(d)
July-August relative humidity (%)
Y = -3.68 (±0.57) X + 154.12 (±16.64),
R^2_{adjusted} = 47.4%, P<0.001
Tree-ring δ^{18}O (‰)
(e)
Reconstruction
Observation
FFT-reconstruction
FFT-observation
Sign test | r | RE
41+/10- | 0.66 | 0.44
< 0.01 | < 0.001
Year

◀**Fig. 3** **a** Tree-ring $\delta^{18}O$ and the associated with measurement uncertainty (SD) and statistical parameters; **b** the corresponding number of trees available for isotopic analyses during each period; **c** the values of Pearson's correlation coefficient (*r*) between the tree-ring $\delta^{18}O$ and climatic variables at the Fuyun meteorological station. The months followed by "*/p*" indicate values from the previous year. *JJA* represents the mean value from June to August of the current growing season. *JA* represents the mean value from July and August of the current growing season. The *dashed lines* indicate the 95 % confidence intervals. *Bars* and *lines* that extend outside these *dashed lines* are statistically significant. **d** The relationship between the July–August relative humidity and the tree-ring $\delta^{18}O$ data (linear regression); **e** comparison of the measured July–August relative humidity with the reconstructed July–August relative humidity, with the uncertainty (SD) depicted in *gray* (see the text for details). The *thick lines* are the 10-year low-pass-filtered values based on a 10-year fast Fourier transform (FFT). The associated verification statistics are provided in the inserted table

Table 1 The partial correlations between the tree-ring $\delta^{18}O$ and the July–August climatic parameters

Controlled variable	$\delta^{18}O$ versus mean $T_{7–8}$	$\delta^{18}O$ versus max $T_{7–8}$	$\delta^{18}O$ versus $Pre_{7–8}$	$\delta^{18}O$ versus $RH_{7–8}$
Mean $T_{7–8}$		0.41**	−0.51**	−0.45**
Max $T_{7–8}$	-0.20^{ns}		−0.42**	−0.37**
$Pre_{7–8}$	0.62**	0.64**		−0.60**
$RH_{7–8}$	0.16^{ns}	0.28*	-0.22^{ns}	

Mean and max $T_{7–8}$ are the mean and maximum July–August temperature, respectively; $Pre_{7–8}$ and $RH_{7–8}$ are the July–August precipitation and relative humidity, respectively

ns not significant

* $P < 0.05$; ** $P < 0.01$

meaningful calibration and verification [40]. We used the sign test, Pearson's *r*, and the reduction of error (RE) to verify the reconstruction [40]. We assessed the spatial representativeness of the reconstruction by conducting a spatial correlation analysis between our reconstruction and the CRU ts3.10.01 dataset [41] using the KNMI Climate Explorer software (http://climexp.knmi.nl). We conducted 30-year negative exponential smoothing and regime-shift analysis to explore the variability of relative humidity during the study period. Moreover, to further validate our reconstruction, we compared it with series for the regional palmer drought severity index (PDSI, [42]), western drought mode for central High Asia [43], and the precipitation mode in the northwestern Xinjiang region of China [44].

3 Results and discussion

3.1 Statistical analysis of the tree-ring $\delta^{18}O$ chronology

The $\delta^{18}O$ in tree rings averaged 29.2 ± 1.0 ‰ (1 σ) (Fig. 3a) since 1790, which is about 8 ‰ higher than the value (21.3 ‰) previously reported for larch (*Larix gmelinii* Rupr.) on the eastern part of the Taimyr Peninsula of Russia [45]. The mean value was about 2 ‰ higher than that of larch (*L. sibirica* Ldb.) in the Russian Altay region [46]. The maximum $\delta^{18}O$ value was 32.5 ‰ (in 1817) and the minimum value was 26.4 ‰ (in 1993). Thus, the range of $\delta^{18}O$ was 6.1 ‰ for the period from 1790 to 2011.

3.2 Tree-ring $\delta^{18}O$ response to climate

We calculated Pearson's correlation coefficients between tree-ring $\delta^{18}O$ and the main climatic parameters. Temperatures (maximum and mean), precipitation, and relative humidity were significantly correlated with tree-ring $\delta^{18}O$ during several periods (Fig. 3c). The maximum and mean temperatures in the previous September and from March to August were significantly positively correlated with the tree-ring $\delta^{18}O$ (Fig. 3c). The correlation coefficients were strongest for the mean and maximum July–August temperatures, reaching 0.61 ($P < 0.01$) and 0.67 ($P < 0.01$), respectively. The monthly minimum temperature was significantly but more weakly correlated with $\delta^{18}O$ in April and May. The tree-ring $\delta^{18}O$ showed significantly negative correlations with July ($r = -0.49$, $P < 0.01$), July–August ($r = -0.48$, $P < 0.01$), and June–July–August ($r = -0.48$, $P < 0.01$) precipitation (Fig. 3c), as well as during the previous September ($r = -0.36$, $P < 0.01$). Tree-ring $\delta^{18}O$ was significantly negatively correlated with the relative humidity from March to October (Fig. 3c), and with the June–July–August ($r = -0.68$, $P < 0.001$) and July–August ($r = -0.70$, $P < 0.001$) relative humidity.

These results indicated that the July–August relative humidity primarily controlled the tree-ring $\delta^{18}O$ variability. We used partial correlation analysis to test this hypothesis (Table 1). The results showed that the July–August relative humidity was also significantly negatively correlated with tree-ring $\delta^{18}O$ when the July–August mean temperature, maximum temperature, and precipitation were controlled separately. The tree-ring $\delta^{18}O$ was weakly positively correlated with the July–August maximum temperature ($r = 0.28$, $P = 0.049$), and was not significantly correlated with the July–August mean temperature and precipitation when the July–August relative humidity was controlled (Table 1).

Tree-ring $\delta^{18}O$ was clearly influenced by relative humidity (Fig. 3c), and similar results were obtained in previous studies [9, 15, 18, 47]. As we indicated in the Introduction, the tree-ring $\delta^{18}O$ model [9, 10, 15, 16] can explain the negative correlations between relative humidity and tree-ring $\delta^{18}O$. When the relative humidity is low, transpiration is high and this increases the $\delta^{18}O$ of leaf water. Lower atmospheric humidity creates a higher vapor-pressure gradient between the leaf's interstitial spaces and the ambient atmosphere, resulting in a preferential loss of lighter isotopes and consequent enrichment of the leaf-water $\delta^{18}O$ [13]. Precipitation also strongly affects the relative humidity, which in turn controls the degree of evaporative enrichment of leaf-water $\delta^{18}O$ [9], and, therefore, tree-ring $\delta^{18}O$. These phenomena can explain the relationships between the tree-ring $\delta^{18}O$ and July and July–August precipitation.

Tree-ring $\delta^{18}O$ was significantly positively correlated with the mean temperature and the maximum temperature during the growing season, which reflects the effects of the temperature on regional moisture conditions. Both temperatures indirectly influence tree-ring $\delta^{18}O$ by changing the moisture conditions (e.g., evaporation and transpiration) during the growing season. The July–August temperature was significantly negatively correlated with the July–August relative humidity ($r = -0.76$, $P < 0.001$, Fig. 2b), which supports our explanation of this pattern. During this period, increasing temperatures stimulate the evaporation of soil water, resulting in a preferential loss of lighter isotopes from the soil water [13], which in turn is taken up by trees as enriched soil water.

Overall, the relative humidity during the growing season is low (mean 45.6 %), and this suggests that relative humidity may be a main limiting factor for fractionation of $\delta^{18}O$ in leaf water. Our results also indicated that the tree-ring $\delta^{18}O$ increases with increasing temperature and with decreasing precipitation and relative humidity (Fig. 3c); thus, it depends strongly on moisture conditions.

3.3 Relative humidity reconstruction

We established a transfer function by means of linear regression to use the July–August relative humidity as the dependent variable and the tree-ring $\delta^{18}O$ as the independent variable based on the results of our analysis of the tree-ring $\delta^{18}O$ response to relative humidity. The final calibration model explained 47.4 % (adjusted R^2; $P < 0.001$) of the total variation in the measured July–August relative humidity from 1961 to 2011 (Fig. 3d). The F value was 46.01, which indicated that the model did a good job of describing the relationship between $\delta^{18}O$ and the July–August relative humidity. Although the Durbin–Watson value was 0.99, no significant linear trend in time series of the residuals was detected.

The tree-ring $\delta^{18}O$ increased at a rate of 3.68 (±0.57) ‰ per 1 % decrease in relative humidity (Fig. 3d). The uncertainties in the reconstruction were estimated using bootstrap methods [37, 38]. Two-thirds of the data (the calibration data) were randomly sampled with replacement; the best linear regression was calculated using this data and the quality of the reconstruction was assessed using the verification samples (the remaining one-third of the data). After 1,000 iterations of this method, we estimated the uncertainty of the model as the mean standard deviation of the verification data (0.99 %). We then determined the total uncertainty of the $\delta^{18}O$ reconstruction in a given year by adding the uncertainty of the $\delta^{18}O$ measurement (the y-intercept of the regression multiplied by the uncertainty of the $\delta^{18}O$ measurement) to the uncertainty of the regression. The mean uncertainty of the relative humidity reconstruction was 1.59 %, which is lower than the range of the observed relative humidity (20.7 %).

The reconstructed relative humidity showed very similar fluctuations to those of the observed relative humidity in both the inter-decadal ($r = 0.61$, $P < 0.001$) and the annual values ($r = 0.70$, $P < 0.001$; Fig. 3e). The results of the leave-one-out method yielded a positive RE (0.44), thus indicating acceptable predictive ability of the regression model. A statistically significant sign test (41 +/10−, $P < 0.01$) and Pearson's correlation coefficient ($r = 0.66$, $P < 0.001$) between the measured values and the leave-one-out-derived estimates also support the validity of the reconstruction (Fig. 3e). The linear model can, therefore, be used to reconstruct variation of the July–August relative humidity since 1790.

The regional relative humidity reflects a balance between thermal conditions and water conditions through the feedback of evaporation and precipitation [1]. Thus, relative humidity provides a good representation of overall hydrological and climatic conditions and of the humidity conditions that affect photosynthesis. Figure 2b shows that the July–August relative humidity showed variability similar to that of the July–August precipitation at annual scale ($r = 0.50$, $P < 0.01$), even though the relative humidity was lower when the precipitation was most abundant during the growing season (Fig. 2a). Owing to a shortage of long-term relative humidity data for our study area, we used the CRU ts3.10.01 precipitation data to validate our reconstruction. The spatial correlation map (Fig. 4) showed that the reconstructed relative humidity was significantly correlated with precipitation variability in western Mongolia, our study area, and eastern Kazakhstan both from 1960 to 2009 and from 1901 to 2009. The spatial correlation pattern between our reconstruction and CRU ts3.10.01 precipitation was similar to the pattern of drought in the western region of High Asia [43].

The spatial correlation coefficient at our sampling site was lower than those for western Mongolia and eastern Kazakhstan (Fig. 4). One reason for this difference may be the fact that more data are available from more meteorological stations in western Mongolia and eastern Kazakhstan in the CRU dataset (http://www.cru.uea.ac.uk/cru/

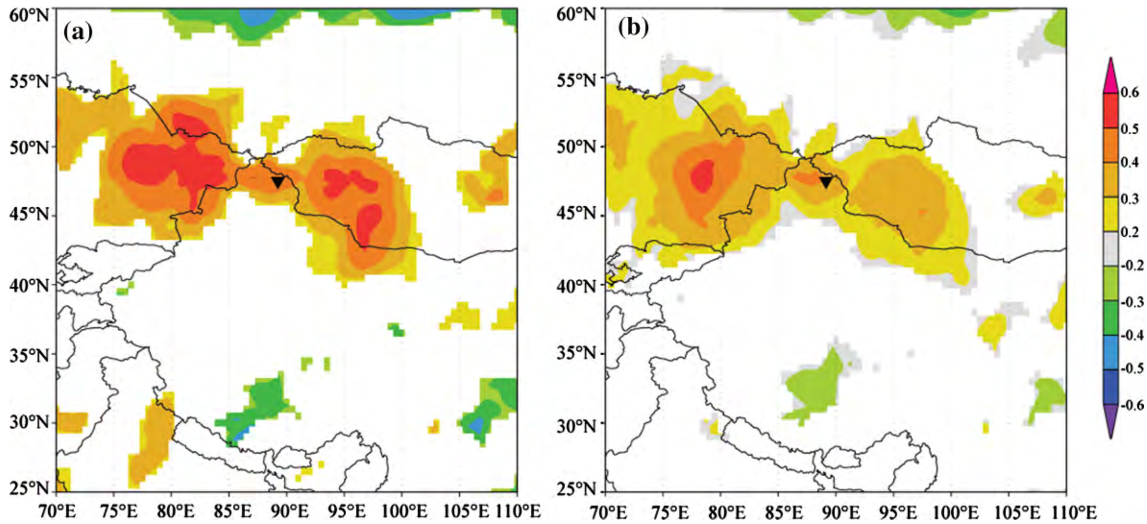

Fig. 4 Patterns of spatial correlation between the reconstruction and the mean values of July–August precipitation data from the regional grid (CRU ts3.10.01, [41]) from **a** 1960–2009 and **b** 1901–2009. Only statistically significant correlations ($P < 0.1$) are shown. The *triangles* indicate the location of the sampling site. The analyses were accomplished using the KNMI Climate Explorer software (Royal Netherlands Meteorological Institute; http://climexp.knmi.nl)

data/landstations/; [41]), whereas only one station was available in our study area. It is also possible that this reflects real discrepancies between the relative humidity and precipitation. Although the spatial correlations between the reconstruction of relative humidity and the CRU ts3.10.01 precipitation data around the sampling site were lower than those farther from the sample site, the spatial correlations were nonetheless statistically significant for our study area. Our results, therefore, suggest that the relative humidity in our study area varied coherently with precipitation along the Altay Mountains.

We used the transfer function to reconstruct the July–August relative humidity since 1790. To test the mean value shift of our relative humidity reconstruction, we conducted a regime-shift analysis using the Regime Shift Detection software V3.2 [48]. Figure 5 shows the long-term variations revealed by negative exponential smoothing using a 30-year moving window; three major shifts are apparent (in 1817, 1830, and 2004). From 1790 to 1830, relative humidity showed a decreasing trend, and a 14-year minimum was observed from 1817 to 1830. From 1830 to 1946, relative humidity fluctuated around the mean values, and a period of higher than average relative humidity appeared from 1946 to the 1990s. After the 1990s, the relative humidity decreased toward a lower value, and a minimum mean value appeared from 2004 to 2011.

We also investigated the extreme years with unusually high or low relative humidity. We defined extreme years as those with a reconstructed relative humidity value that exceeded the regime-shift mean value and 1.5 σ of the whole series (the dotted lines in Fig. 5). These extremes are represented by upward (high) and downward (low) bars in Fig. 5b. In total, we detected 18 extreme years, which accounted for about 8 % of the 222 years in our study period. Two-thirds of the extreme years occurred during the 20th century, and most were detected from 1946 to the 1990s.

3.4 Validation of the reconstruction

(i) Reconstruction of other moisture parameters based on tree-ring data. Several moisture-sensitive tree-ring reconstructions (drought and precipitation) from areas near our study area provide references that can be used to validate our reconstruction. Our reconstruction agrees well with the PDSI reconstruction near the sampling site (4 grid points, from 46.25° to 48.75°N, and from 88.75° to 91.25°E) from the Monsoon Asia Drought Atlas (MADA) [42] with correlation coefficients ranging from 0.31 to 0.43 ($P < 0.01$, $n = 216$). We averaged the PDSI data from the four corners of the MADA area to provide a regional PDSI reconstruction from 1790 to 2005. Our reconstruction showed variability consistent with the regional PDSI at annual ($r = 0.39$, $P < 0.01$) and decadal scales ($r = 0.37$, $P < 0.01$) (Fig. 6a, b). The reconstruction also showed similar fluctuations with the western mode of drought in central High Asia from 1790 to 1992 [43] at annual ($r = 0.25$, $P < 0.01$) and decadal scales ($r = 0.27$, $P < 0.01$), and with a spatial point-by-point precipitation reconstruction in northwestern China from 1803 to 1990 [44] at annual ($r = 0.32$, $P < 0.01$) and decadal scales ($r = 0.35$, $P < 0.01$) (Fig. 6a, c, d). This coherent

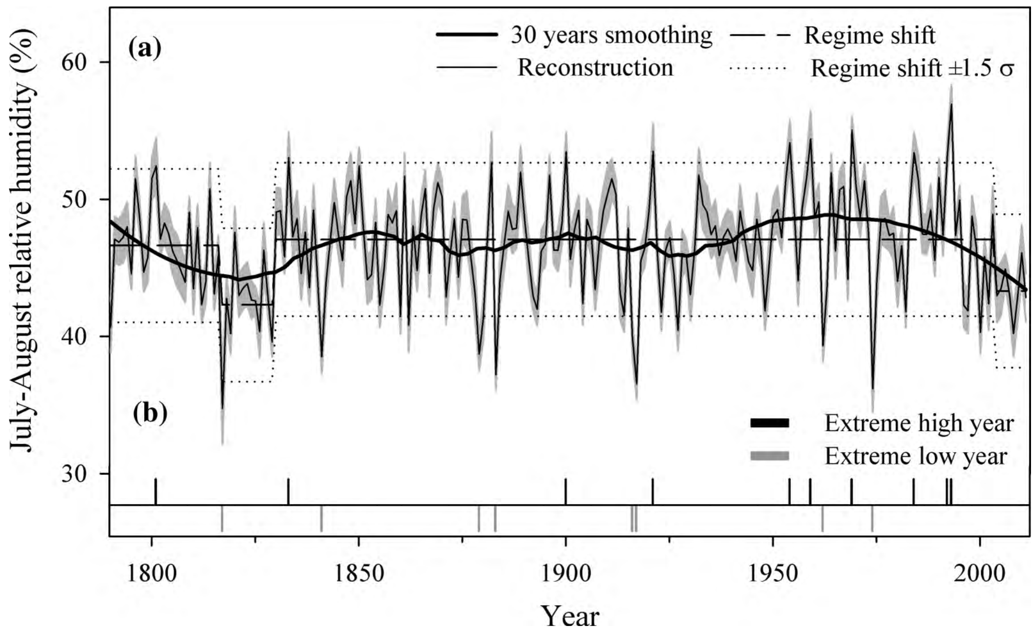

Fig. 5 **a** Reconstructed July–August relative humidity and the associated regime shifts. The *thin black line* is the reconstructed PDSI, with its associated uncertainty (SD) shown in *gray* (see the text for details), and the *dashed line* represent the regime shifts (cutoff length = 10 years; *dotted lines*, 95 % confident intervals); the *thick black line* represents the 30-year negative exponential smoothing of the reconstructed relative humidity. **b** The *black* and *gray bars* correspond to extremely wet or dry (respectively) years (with values exceeding 1.5 σ different from the rest of the series)

variability also agrees with the spatial correlation patterns (Fig. 4). The 31-year moving-window correlation analyses provided positive correlations between this reconstruction and other reconstructions during most periods, and significant correlations appeared from 1805 to 1840 and after 1940 (Fig. 6e). In the long term, the reconstructed relative humidity showed fluctuations similar to those of other moisture parameter reconstructions. This suggests that that the reconstructed relative humidity can be used as a parameter that reveals drought conditions.

However, some differences existed among the different reconstructions during short intervals. For example, from 1840 to 1860 and from 1900 to 1930, our reconstruction (Fig. 6a) showed not only fluctuations similar to those in the precipitation reconstruction (Fig. 6d), but also some differences from the MADA PDSI and western mode drought reconstruction (Fig. 6b, c). The 31-year moving correlation coefficients were also low and not significant during those periods (Fig. 6e). These discrepancies may have been caused by differences in moisture parameters such as precipitation, relative humidity, and PDSI and by the different signal window. For example, the reconstructed relative humidity is from July to August, while the precipitation reconstruction is from January to October and the PDSI reconstruction is from June to August. These discrepancies may also have been caused by the differences between site-specific and regional reconstructions. However, the relative humidity reconstruction is robust. This result suggests that different moisture parameters should be available in efforts to access the regional drought variability.

(ii) The 1817–1830 and 2004–2011 anomalies. We focused on the regime shifts observed from 1817 to 1830 and from 2004 to 2011, which had the lowest relative humidity during our study period. In a spatial drought reconstruction for central High Asia [43] and a precipitation reconstruction for northwestern China [44], the period from 1817 to 1830 also had a drier climate. The extreme drought events were significantly drier than the mean in 1829 throughout the entire Xinjiang area of China [44]. A relatively dry period in the 1820s was also reported in the central Tianshan Mountains [49]. Mongolia also experienced drought conditions from 1821 to 1825 [50], and the southeastern Tibetan Plateau had drier conditions from 1807 to 1817 [51].

Another dry regime-shift mean value appeared from 2004 to 2011 after a trend of decreasing relative humidity after the 1990s (Fig. 5). This trend was confirmed using actual July–August precipitation and relative humidity values for the study area (Fig. 2b). Similarly, several droughts occurred in Mongolia from 1999 to 2005 [50] and in China from the 1900s to 2001 [52]. The regional MADA PDSI reconstruction also showed decreasing moisture during the late 1990s (Fig. 6b). Similar abnormally dry conditions from 1993 to 2003 were reported in the

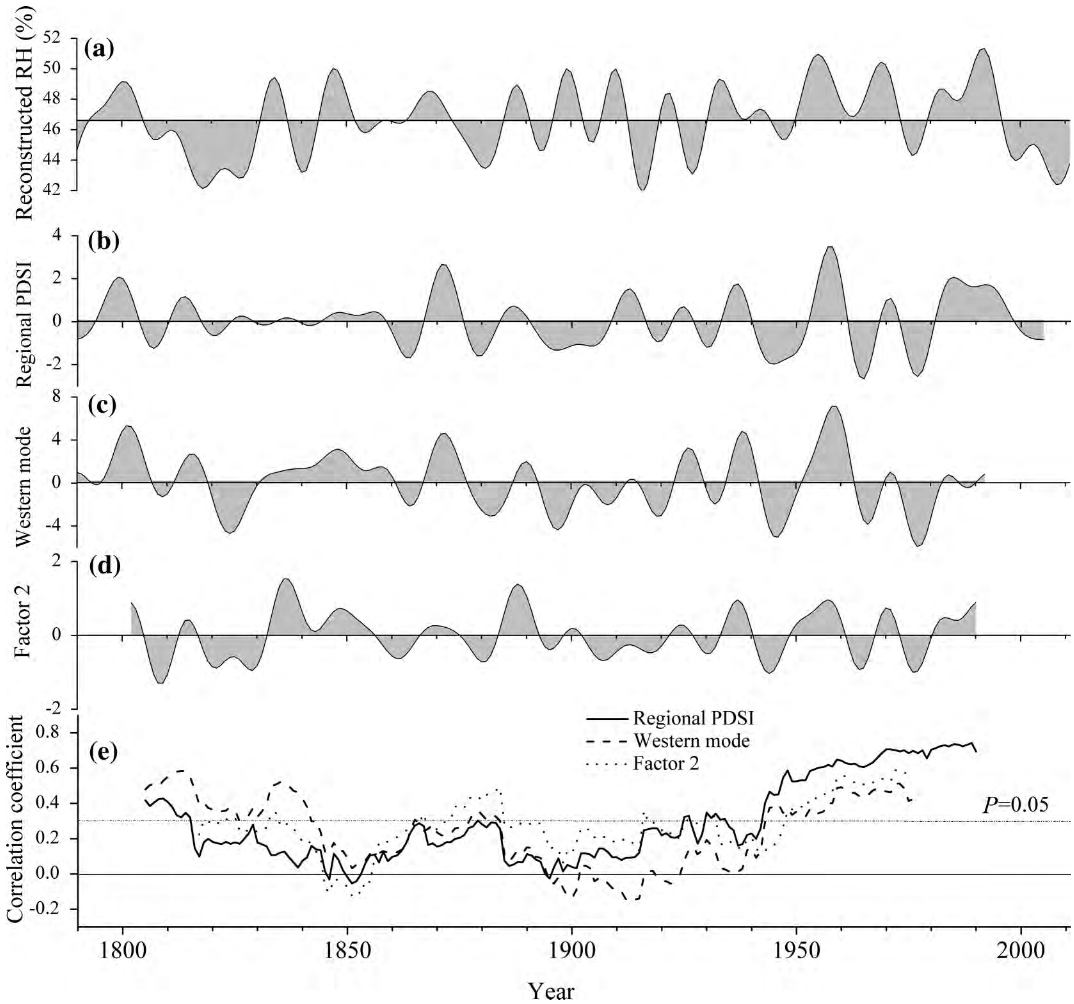

Fig. 6 Comparisons between **a** the present relative humidity reconstruction and **b** the regional June to August (JJA) gridded data near our sampling site from the MADA PDSI dataset [42]; **c** the western drought mode for central High Asia [43]; **d** the normalized score of factor 2 of the precipitation reconstruction (from January to October) for northwestern China [44]; **e** the running correlation between our reconstruction and **b**–**d** at an annual resolution based on a 31-year moving window. The *central horizontal lines* in **a**–**d** represent the long-term mean value. The *gray shaded areas* are the 10-year low-pass-filtered values based on a 10-year fast Fourier transform (FFT)

Xinglong Mountains, in the eastern part of northwestern China [53]. The Ortindag Sand Land, in China's Inner Mongolia region, has also experienced severe sustained droughts during the past 40 years [54]. A large-scale drought event was detected in 2001 in Mongolia, China, Myanmar, and northern Thailand [50]. This revealed that the anomaly from 2004 to 2011 was widespread, not just confined to the Altay Mountains of northwestern Xinjiang region.

(iii) Northwestern Xinjiang moisture conditions in the 20th century. The relative humidity reconstruction showed an increasing trend from 1900 to the 1990s, even though it was interrupted by several short periods with low values. Relative humidity was relatively high from 1946 to the 1990s (Fig. 6a). This indicated that the climate in the northwestern Xinjiang was relatively wet during the last half of the 20th century. Other moisture records suggest that this was a more widespread signal. A relatively wet period during the 1950s can be seen in the regional MADA PDSI reconstruction (Fig. 6b), in the western drought mode in central High Asia (Fig. 6c), and for precipitation in northwestern Xinjiang region (Fig. 6d). The regional MADA PDSI reconstruction also showed a wet climate from 1980 to the 1990s, which was similar to our reconstruction. The trend of wetting during the last half of the 20th century in study area was also confirmed by the measured precipitation data from 1951 to the 1990s [55]. Treydte et al. [56] reported that precipitation was highest in northern Pakistan during the 20th century. Li et al. [49] also pointed out that there was a trend of increasing moisture in the central Tianshan Mountains during the 20th century. The wettest period occurred in the mid-1990s in western Mongolia [50]. A wetting trend from the 1980s to the 1990s was also supported by an analysis of several proxies [57], although this trend seems to have reserved after the 1990s (Fig. 6a).

4 Conclusions

In this paper, we describe a robust 222-year reconstruction of the July–August relative humidity based on tree-ring $\delta^{18}O$ data from the Altay Mountains of northwestern China. Two regime-shift periods with lower relative humidity have appeared since 1790: one from 1817 to 1830 and another from 2004 to 2011. From 1830 to 1946, the relative humidity was relatively stable. From 1900 to the 1990s, the relative humidity showed an initially increasing trend followed by a downward trend after the 1990s. Most of the years with extremely wet or dry conditions were concentrated in the 20th century, and most of these periods occurred from 1946 to the 1990s. The reconstructed relative humidity showed variability consistent with the long-term regional moisture trends, despite some discrepancies. Our results, therefore, suggest the possibility of using long-term relative humidity data to assess evapotranspiration and the water and energy balance and fluxes in climate models.

Acknowledgments The authors thank the anonymous reviewers and editors for their constructive comments and suggestions. This work was supported by the Global Change Research Program of China (2010CB951401), the National Natural Science Foundation of China (41171167), the Project for Incubation of Specialists in Glaciology and Geocryology of the National Natural Science Foundation of China (J0930003/J0109), the China Desert Meteorological Science Research Foundation (Sqj2011013 and Sqj2009001), the Chinese Academy Science Special Grant for Postgraduate Research, Innovation and Practice, and the Chinese Academy of Sciences Interdisciplinary Innovation Team Project (29Y329B91).

References

1. Sherwood SC, Ingram W, Tsushima Y et al (2010) Relative humidity changes in a warmer climate. J Geophys Res 115(D9): D09104. doi:10.1029/2009JD012585
2. Zuo HC, Li DL, Hu YQ et al (2005) Characteristics of climatic trends and correlation between pan-evaporation and environmental factors in the last 40 years over China. Chin Sci Bull 50:1235–1241
3. Rawson H, Begg J, Woodward R (1977) The effect of atmospheric humidity on photosynthesis, transpiration and water use efficiency of leaves of several plant species. Planta 134:5–10
4. Osonubi O, Davies W (1980) The influence of plant water stress on stomatal control of gas exchange at different levels of atmospheric humidity. Oecologia 46:1–6
5. Hovenden MJ, Vander Schoor JK, Osanai Y (2012) Relative humidity has dramatic impacts on leaf morphology but little effect on stomatal index or density in *Nothofagus cunninghamii* (Nothofagaceae). Aust J Bot 60:700–706
6. Hoffman GJ, Rawlins SL, Garber MJ et al (1971) Water relations and growth of cotton as influenced by salinity and relative humidity. Agron J 63:822–826
7. Spomer LA, Tibbitts TW (1997) Humidity. In: Langhans RW, Tibbitts TW (eds) Plant growth chamber handbook. Iowa State University, Ames, pp 43–64
8. Krug BA, Whipker BE, McCall I et al (2013) Elevated relative humidity increases the incidence of distorted growth and boron deficiency in bedding plant plugs. HortScience 48:311–313
9. Roden JS, Lin G, Ehleringer JR (2000) A mechanistic model for interpretation of hydrogen and oxygen isotope ratios in tree-ring cellulose. Geochim Cosmochim Acta 64:21–35
10. McCarroll D, Loader NJ (2004) Stable isotopes in tree rings. Quat Sci Rev 23:771–801. doi:10.1016/j.quascirev.2003.06.017
11. Dongmann G, Nürnberg HW, Förstel H et al (1974) On the enrichment of $H_2^{18}O$ in the leaves of transpiring plants. Radiat Environ Biophys 11:41–52
12. Liu Y, Cai QF, Liu WG et al (2008) Monsoon precipitation variation recorded by tree-ring $\delta^{18}O$ in arid northwest China since AD 1878. Chem Geol 252:56–61
13. Sano M, Ramesh R, Sheshshayee M et al (2012) Increasing aridity over the past 223 years in the Nepal Himalaya inferred from a tree-ring $\delta^{18}O$ chronology. Holocene 22:809–817
14. Gessler A, Löw M, Heerdt C et al (2009) Within-canopy and ozone fumigation effects on $\delta^{13}C$ and $\Delta^{18}O$ in adult beech (*Fagus sylvatica*) trees: relation to meteorological and gas exchange parameters. Tree Physiol 29:1349–1365
15. Waterhouse JS, Switsur VR, Barker AC et al (2002) Oxygen and hydrogen isotope ratios in tree rings: how well do models predict observed values? Earth Planet Sci Lett 201:421–430
16. Sternberg LSL (2009) Oxygen stable isotope ratios of tree-ring cellulose: the next phase of understanding. New Phytol 181: 553–562
17. Shu Y, Feng XH, Gazis C et al (2005) Relative humidity recorded in tree rings: a study along a precipitation gradient in the Olympic Mountains, Washington, USA. Geochim Cosmochim Acta 69:791–799
18. Tsuji H, Nakatsuka T, Takagi K (2006) $\delta^{18}O$ of tree-ring cellulose in two species (spruce and oak) as proxies of precipitation amount and relative humidity in northern Japan. Chem Geol 231:67–76
19. Yapp CJ, Epstein S (1982) A reexamination of cellulose carbon-bound hydrogen δD measurements and some factors affecting plant-water D/H relationships. Geochim Cosmochim Acta 46: 955–965
20. Edwards TWD, Fritz P (1986) Assessing meteoric water composition and relative humidity from ^{18}O and ^{2}H in wood cellulose: paleoclimatic implications for southern Ontario, Canada. Appl Geochem 1:715–723
21. Wright WE, Leavitt SW (2006) Boundary layer humidity reconstruction for a semiarid location from tree ring cellulose $\delta^{18}O$. J Geophys Res 111:D18105. doi:10.1029/2005jd006806
22. Tsuji H, Nakatsuka T, Yamazaki K et al (2008) Summer relative humidity in northern Japan inferred from $\delta^{18}O$ values of the tree ring in (1776–2002 A.D.): influence of the paleoclimate indices of atmospheric circulation. J Geophys Res 113(D18):D18103. doi:10.1029/2007jd009080
23. Wang WZ, Liu XH, Xu GB et al (2013) Moisture variations over the past millennium characterized by Qaidam Basin tree-ring $\delta^{18}O$. Chin Sci Bull. doi:10.1007/s11434-013-5913-0
24. Khaliq MN, Ouarda TBMJ (2007) On the critical values of the standard normal homogeneity test (SNHT). Int J Climatol 27: 681–687
25. Abaimov AP (2010) Geographical distribution and genetics of Siberian larch species. In: Osawa A, Zyryanova OA, Matsuura Y et al (eds) Permafrost ecosystems. Springer, Amsterdam, pp 41–58

26. Zhou WS, Li JF, Zhang ZJ (1989) Some problems in developing the tree-ring chronologies in the south slope of the Altay mountain (in Chinese). In: Li JF, Zhagn ZJ, Yuan YJ (eds) Study of tree-ring climatology and tree-ring hydrology in Xinjiang. Meteorological Press, Beijing, pp 9–17
27. Li JF, Yuan YJ (1989) Effect of snow on the growth of tree-ring (in Chinese). In: Li JF, Zhagn ZJ, Yuan YJ (eds) Study of tree-ring climatology and tree-ring hydrology in Xinjiang. Meteorological Press, Beijing, pp 87–91
28. Stokes MA, Smiley TL (1968) An introduction of tree-ring dating. University of Chicago, Chicago
29. Holmes RL (1983) Computer-assisted quality control in tree-ring dating and measurement. Tree-ring Bull 43:69–78
30. Daux V, Edouard JL, Masson-Delmotte V et al (2011) Can climate variations be inferred from tree-ring parameters and stable isotopes from *Larix decidua*? Juvenile effects, budmoth outbreaks, and divergence issue. Earth Planet Sci Lett 309:221–233
31. Young GHF, Demmler JC, Gunnarson BE et al (2011) Age trends in tree ring growth and isotopic archives: a case study of *Pinus sylvestris* L. from northwestern Norway. Glob Biogeochem Cycles 25(2):GB2020. doi:10.1029/2010gb003913
32. Leavitt SW (2008) Tree-ring isotopic pooling without regard to mass: no difference from averaging $\delta^{13}C$ values of each tree. Chem Geol 252:52–55
33. Liu XH, Shao XM, Liang EY et al (2009) Climatic significance of tree-ring $\delta^{18}O$ in the Qilian Mountains, northwestern China and its relationship to atmospheric circulation patterns. Chem Geol 268:147–154
34. Loader NJ, Robertson I, Switsur VR et al (1997) An improved technique for the batch processing of small whole wood samples to α-cellulose. Chem Geol 136:313–317
35. Liu XH, Liu Y, Xu GB et al (2010) Pretreatment of the tree-ring samples for stable isotope analysis. J Glaciol Geocryol 32:1242–1250 (in Chinese)
36. Laumer W, Andreu L, Helle G et al (2009) A novel approach for the homogenization of cellulose to use micro-amounts for stable isotope analyses. Rapid Commun Mass Spec 23:1934–1940
37. Davison AC, Hinkley DV (1997) Bootstrap methods and their application. Cambridge University, Cambridge
38. Wigley T, Briffa K, Jones P (1984) On the average value of correlated time series, with applications in dendroclimatology and hydrometeorology. J Clim Appl Meteorol 23:201–213
39. Michaelsen J (1987) Cross-validation in statistical climate forecast models. J Clim Appl Meteorol 26:1589–1600
40. Fritts HC (1976) Tree rings and climate. Academic Press, London
41. Mitchell TD, Jones PD (2005) An improved method of constructing a database of monthly climate observations and associated high-resolution grids. Int J Climatol 25:693–712
42. Cook ER, Anchukaitis KJ, Buckley BM et al (2010) Asian monsoon failure and megadrought during the last millennium. Science 328:486–489
43. Fang KY, Davi N, Gou XH et al (2010) Spatial drought reconstructions for central High Asia based on tree rings. Clim Dynam 35:941–951
44. Fang KY, Gou XH, Chen FH et al (2011) Large-scale precipitation variability over northwest China inferred from tree rings. J Clim 24:3457–3468
45. Sidorova OV, Siegwolf RTW, Saurer M et al (2010) Spatial patterns of climatic changes in the Eurasian north reflected in Siberian larch tree-ring parameters and stable isotopes. Glob Change Biol 16:1003–1018
46. Sidorova O, Saurer M, Myglan V et al (2012) A multi-proxy approach for revealing recent climatic changes in the Russian Altai. Clim Dyn 38:175–188
47. Robertson I, Waterhouse JS, Barker AC et al (2001) Oxygen isotope ratios of oak in east England: implications for reconstructing the isotopic composition of precipitation. Earth Planet Sci Lett 191:21–31
48. Rodionov SN (2006) Use of prewhitening in climate regime shift detection. Geophys Res Lett 33:L12707. doi:10.1029/2006GL025904
49. Li JB, Gou XH, Cook ER et al (2006) Tree-ring based drought reconstruction for the central Tien Shan area in northwest China. Geophys Res Lett 33:L07715. doi:10.1029/2006gl025803
50. Davi N, Jacoby G, Fang KY et al (2010) Reconstructing drought variability for Mongolia based on a large-scale tree ring network: 1520–1993. J Geophys Res 115:D22103. doi:10.1029/2010JD013907
51. Shi CM, Daux V, Zhang QB et al (2012) Reconstruction of southeast Tibetan plateau summer climate using tree ring $\delta^{18}O$: moisture variability over the past two centuries. Clim Past 8:205–213
52. Li JB, Cook E, D'arrigo R et al (2009) Moisture variability across China and Mongolia: 1951–2005. Clim Dyn 32:1173–1186
53. Fang KY, Gou XH, Chen FH et al (2009) Drought variations in the eastern part of northwest China over the past two centuries: evidence from tree rings. Clim Res 38:129–135
54. Liang EY, Shao XM, Liu HY et al (2007) Tree-ring based PDSI reconstruction since AD 1842 in the Ortindag Sand Land, east Inner Mongolia. Chin Sci Bull 52:2715–2721
55. Zou XK, Zhai PM, Zhang Q (2005) Variations in droughts over China: 1951–2003. Geophys Res Lett 32:L04707. doi:10.1029/2004GL021853
56. Treydte KS, Schleser GH, Helle G et al (2006) The twentieth century was the wettest period in northern Pakistan over the past millennium. Nature 440:1179–1182
57. Shi YF, Shen YP, Kang ES et al (2007) Recent and future climate change in northwest China. Clim Change 80:379–393